B-Doped Pd Catalyst: Boosting Room-Temperature Hydrogen Production from Formic Acid-Formate Solutions

ARTICLE *in* JOURNAL OF THE AMERICAN CHEMICAL SOCIETY · MARCH 2014

Impact Factor: 12.11 · DOI: 10.1021/ja5008917 · Source: PubMed

4 AUTHORS, INCLUDING:

Shouzhong Zou
American University Washington D.C.
74 PUBLICATIONS **2,440** CITATIONS

SEE PROFILE

Wen-Bin Cai
Fudan University
111 PUBLICATIONS **2,113** CITATIONS

SEE PROFILE

JACS
JOURNAL OF THE AMERICAN CHEMICAL SOCIETY
Communication
pubs.acs.org/JACS

B-Doped Pd Catalyst: Boosting Room-Temperature Hydrogen Production from Formic Acid–Formate Solutions

Kun Jiang,[†] Ke Xu,[†] Shouzhong Zou,[‡] and Wen-Bin Cai*[,†]

[†]Shanghai Key Laboratory of Molecular Catalysis and Innovative Materials, Collaborative Innovation Center of Chemistry for Energy Materials, Department of Chemistry, Fudan University, Shanghai 200433, China

[‡]Department of Chemistry and Biochemistry, Miami University, Oxford, Ohio 45056, United States

Supporting Information

ABSTRACT: Facile production of hydrogen at room temperature is an important process in many areas including alternative energy. In this Communication, a potent boron-doped Pd nanocatalyst (Pd-B/C) is reported for the first time to boost hydrogen generation at room temperature from aqueous formic acid–formate solutions at a record high rate. Real-time ATR-IR spectroscopy is applied to shed light on the enhanced catalytic activity of B-doping and reveals that the superior activity of Pd-B/C correlates well with an apparently impeded CO_{ad} accumulation on its surfaces. This work demonstrates that developing new anti-CO poisoning catalysts coupled with sensitive interfacial analysis is an effective way toward rational design of cost-effective catalysts for better hydrogen energy exploitation.

Hydrogen storage and production are of great importance for the exploitation of sustainable and renewable energies to meet environmental and socio-economic concerns, in consideration of its abundant supply and its clean and efficient utilization, especially in low-temperature fuel cells. For safe and convenient handling, various hydrogen storage chemicals have been considered to replace classic pressurization or cryogenic liquefaction technology.[1,2]

Among these chemicals, formic acid (FA) is regarded as most promising because it is an avirulent nonflammable liquid and a natural biomass and can be produced from CO_2 reduction.[3,4] It is known that the chemical decomposition of FA proceeds via two main pathways, i.e., the dehydrogenation pathway to form H_2 and CO_2, and the dehydration pathway to form H_2O and CO (Scheme 1).[4] The reactivity and selectivity of these two pathways are strongly dependent on the catalysts used.[5] For the sake of hydrogen production, it is obviously desirable to develop novel catalysts for efficient FA dehydrogenation.

Scheme 1. Two Main Pathways for Formic Acid Decomposition and the Interconnection of Corresponding Products by Water–Gas Shift Reaction (WGSR) at Elevated Temperatures

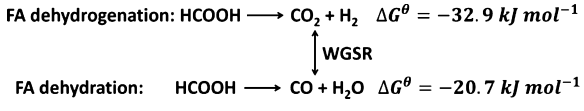

Both homogeneous and heterogeneous catalysts for FA dehydrogenation have been developed.[1,6] Heterogeneous catalysis has the advantage of operating at lower temperatures as well as facile catalyst separation and recycling. Pt, Au, and Pd are primary catalytic metals in heterogeneous catalysis.[7] Among these metals, Pt and Au are much more expensive than Pd. Furthermore, Pt without surface modification or alloying tends to suffer severe CO poisoning from FA dehydration,[8,9] and for Au, a high catalytic activity can only be obtained on subnanometric clusters supported on selected metal oxides, which is not trivial in scale-up synthesis.[10,11] In this regard, Pd-based nanocatalysts are most attractive for practical hydrogen production from FA-containing solutions.[12−16] Nevertheless, the catalysts reported so far are mainly limited to Pd alloyed with a coinage metal like Au or Ag[17−22] or core–shell structured Ag@Pd,[23] calling for new, efficient catalysts at reduced cost.

Despite the increasing interest in heterogeneous catalytic hydrogen production from FA-containing solutions, little effort has been devoted to correlating the performance of a catalyst with the dynamic adsorption at the solid/liquid interface, as has been done at the solid/gas interface.[24] Such knowledge is essential for better understanding the structure–activity relationships as well as for rationally designing potent catalysts. State-of-the-art gas chromatography (GC) and/or transmission FTIR methods can only provide a composition analysis of the gas produced,[22,23,25−27] being unable to monitor the evolution of interfacial species.

Inspired by our previous work on the deactivation mechanism of FA electro-oxidation on Pd electrodes,[28,29] we report here a new class of Pd-based catalysts, i.e., a boron-doped Pd catalyst (Pd-B/C) with a significantly enhanced activity toward hydrogen production from a mixed solution of FA and sodium formate (SF) at room temperature as compared to the commonly used Pd/C synthesized with a $NaBH_4$ reduction method. In fact, turnover frequency (TOF) achieved with this catalyst even surpasses that obtained with a Pd/Au or Pd/Ag catalyst. Equally importantly, we demonstrate that high-sensitivity attenuated total reflection infrared spectroscopy (ATR-IR) can be used to monitor dynamically the interfacial species on Pd-B/C or Pd/C in FA-SF solutions to provide a molecular-level understanding of different activities of the examined catalysts.

Received: January 26, 2014
Published: March 17, 2014

dx.doi.org/10.1021/ja5008917 | J. Am. Chem. Soc. 2014, 136, 4861−4864

Pd/C and Pd-B/C catalysts with a Pd loading of 5 wt% were synthesized through wet chemical reduction of $NaBH_4$ and dimethylamine borane (DMAB), respectively (see Supporting Information for details). TEM images for these as-prepared catalysts are shown in Figure 1. ICP-AES results show that ca. 6 at.% boron is incorporated into Pd-B/C, while the boron content in Pd/C-$NaBH_4$ is less than 3 at.%.

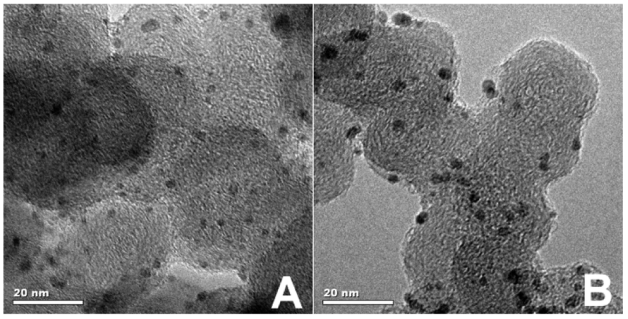

Figure 1. TEM images for 5 wt% (A) Pd/C and (B) Pd-B/C catalysts. The scale bars are 20 nm.

Figure 2 shows the volumes of gas generated from 10 mL solution of 1.1 M FA + 0.8 M SF (pH 3.5, around the pK_a of

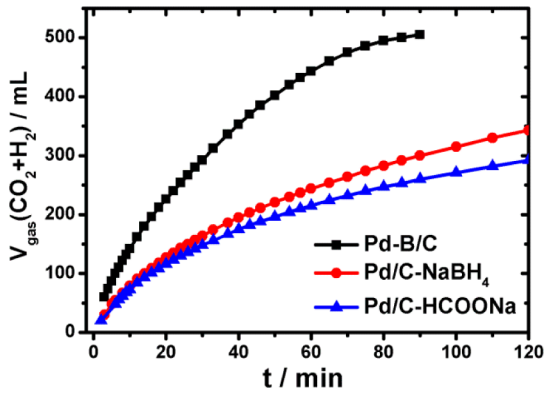

Figure 2. Time-course of reforming gas generation from 10 mL solution of 1.1 M FA + 0.8 M SF in the presence of 100 mg of Pd-based/C (5 wt% Pd) catalysts at 30 °C under ambient atmosphere.

FA) as a function of time with different Pd-based/C catalysts. To exclude any boron doping, HCOONa was used as the reducing agent instead of the commonly used $NaBH_4$ to synthesize Pd/C-HCOONa.[15] Only a slightly higher gas production rate was observed on Pd/C-$NaBH_4$ than on Pd/C-HCOONa, suggesting a poor B-doping, if any, from borohydride. In contrast, the gas production rate is nearly doubled on Pd-B/C as compared to the other two catalysts at a given mass of Pd. After calibration of the sizes of nanocatalysts (i.e., ca. 4.1 nm for Pd-B/C and ca. 2.2 nm for Pd/C-$NaBH_4$), the TOF over the initial 15 min is calculated to be 1184 h^{-1} on Pd-B/C, nearly 4 times that on Pd/C-$NaBH_4$ (304 h^{-1}), suggesting a much higher activity from significant B-doping. Furthermore, compared to the TOF values reported so far for various Pd-based catalysts in FA-SF solutions, i.e., Pd/MSC-30 (750 h^{-1} at 298 K),[30] Pd-NH_2/MIL-125 (214 h^{-1} at 305 K),[31] Pd-Au-Dy/C (470 h^{-1} at 365 K),[18] and Pd_9Ag_1/rGO (526 h^{-1} at 298 K),[32] the present Pd–B/C catalyst show superior catalytic activity. As illustrated in our previous work on FA electro-oxidation, B atoms may be incorporated into Pd–Pd inter-lattice spaces, leading to a slight expansion of Pd lattice, and serving as electron donors to optimize the electronic structure of Pd atoms for FA dehydrogenation.[33,34] In XPS spectra (Figure S1), the Pd^0 $3d_{5/2}$ core-level binding energy for Pd–B/C is slightly upshifted with respect to the reference value for Pd, while that for Pd/C-$NaBH_4$ is virtually unshifted, indicating an effective electron transfer from B to Pd in the former (for more explanations on electron transfer direction, see Supporting Information).[34,35] More catalytic evaluations on as-prepared Pd-B/C, Pd/C, and Pd_3Au/C[12] (at a constant Pd loading of 5 wt%) were also carried out at inclement condition, i.e., with 9.9 M FA + 3.3 M SF at 92 °C, as shown in Figure S2. It turns out that Pd-B/C yields the largest volume of the reforming gas within 150 min, and a rate of ca. 186 mL·min^{-1}·g^{-1} Pd after 2 h, superior to Pd_3Au/C but at a lower cost. The catalytic performance of Pd-B/C may be further improved through structural optimization of the carbon support, according to previous investigations on Pd/C.[30,31]

GC measurement with a thermal conductivity detector (TCD) was performed to analyze the composition of the above reforming gas (Figure 3). The volumetric ratio of H_2 to CO_2 is

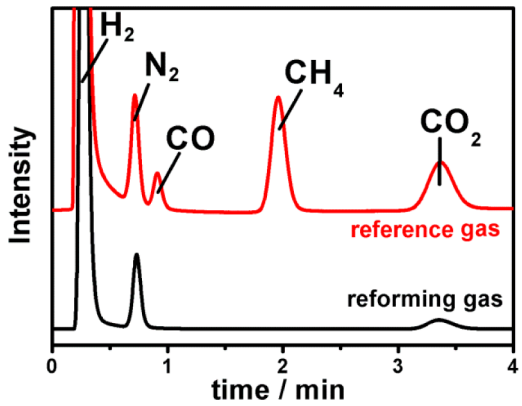

Figure 3. Gas chromatograms of the reforming gas and a reference gas recorded on a GC-TCD.

around 0.9:1 in the above open system (a slightly higher volume of CO_2 may come from the ambient air), arguing against the speculation of a significant contribution from the formate hydrolysis to hydrogen output.[15] Furthermore, no gaseous CO signal was detected in all cases by GC recorded with a methanator and a flame ionization detector (see Figure S3), suggesting that its presence (if any) is lower than the detection limit of 1 ppm. The absence of detectable CO in the generated gas can be associated with a low operation temperature. Otherwise, at elevated temperatures, CO gas would be produced through water–gas shift reaction (Scheme 1).

To better understand the roles of FA and SF in the mixed solution, a control experiment of time-course of Pd-catalyzed gas production from 1.1 M FA, 1.1 M FA + 0.8 M SF, or 1.9 M FA was carried out over Pd/C-$NaBH_4$ at 30 °C. It is clearly seen from Figure 4A that the presence of formate ions in the solution significantly accelerates the hydrogen production rate, as in the case of homogeneous catalysis,[24,25] whereas the initial concentration of FA has far less influence. Nevertheless, gas production from 0.8 M SF alone was too little to be measured, suggesting a negligible contribution from direct formate hydrolysis ($HCOO^- + H_2O \rightarrow H_2 + HCO_3^-$).[30] Adsorbed formate was suggested either to induce a favorable adsorption

dx.doi.org/10.1021/ja5008917 | J. Am. Chem. Soc. 2014, 136, 4861–4864

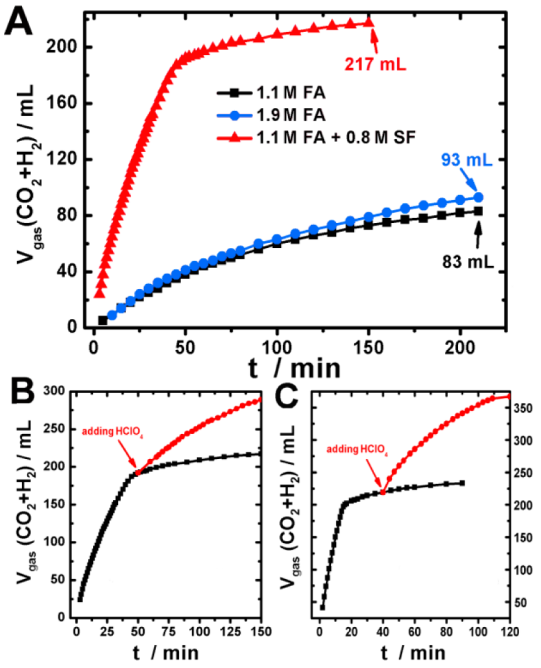

Figure 4. (A) Time-course of reforming gas generation from 5 mL of different solutions in the presence of 100 mg of Pd/C-$NaBH_4$ catalyst at 30 °C under ambient atmosphere. (B,C) Gas generation over 100 mg of Pd/C-$NaBH_4$ (B) or Pd-B/C (C) catalyst in 5 mL of 1.1 M FA + 0.8 M SF with (red) or without (black) addition of 5.5 mmol of $HClO_4$.

orientation of FA (H-down) on the catalyst to promote FA dehydrogenation[36,37] or to act as a reactive intermediate for FA dehydrogenation.[38,39] Also noted is the presence of an inflection point for the 5-mL FA-SF solution with a faster gas production (or a faster consumption of FA) before this point (ca. 81% FA was consumed at t = 50 min). To further understand this, aliquots of $HClO_4$ solution were added to supply hydrogen (or FA). A surge of hydrogen gas production can be seen from Figure 4B. These results suggest that formate ions promote FA dehydrogenation and the inflection point arises when FA in the solution is exhausted. Similar catalytic behavior was observed on Pd-B/C, albeit the inflection point appeared at a much shorter time (ca. 15 min, Figure 4C), reinforcing the superior catalytic activity of Pd-B/C. It should be pointed out that this is the first report regarding a metalloid-doped nanocatalyst for hydrogen generation from FA decomposition.

In order to provide insight into the improved catalytic performance of the Pd-B/C, time-evolved ATR-IR measurements on Pd/C-$NaBH_4$ and Pd-B/C were performed in the FA-SF solution (see Scheme S1 and Figure S4). The strong bands at 1584, 1384, and 1351 cm^{-1} in Figure 5 can be assigned to the solution formate, and a bulk FA peak appears at 1720 cm^{-1}. Augmentation of the bulk signals within the initial 30 s arises from the diffusion of the FA-SF solution to the catalyst surface following its injection. The CO_2 produced (together with H_2 production in the FA dehydrogenation) and dissolved in the solution can be identified from the weak band at 2345 cm^{-1}. A band at 1430 cm^{-1} due to HCO_3^-/CO_3^{2-} can also be clearly observed after 600 s. For comparison, the ATR-IR spectra of aqueous FA, SF, and their mixture on a bare Si prism, as well as the spectra of CO_{ad} on Pd-B/C and Pd/C-$NaBH_4$, are included in Figures S5 and S6.

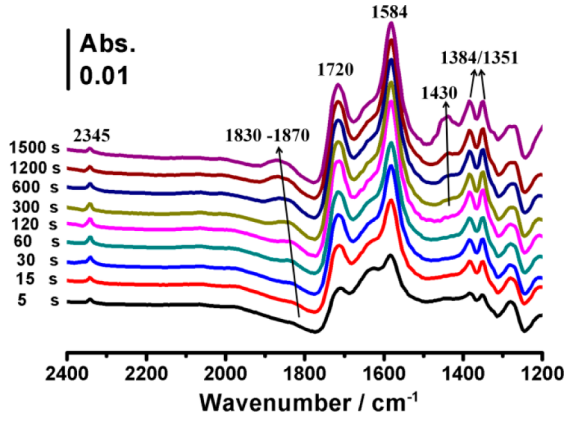

Figure 5. Selected ATR-IR spectra on Pd-B/C catalyst recorded after injection of a premixed 1.1 M FA + 0.8 M SF solution to the spectral cell. The reference spectrum was recorded in air before the injection. The band around 1280 cm^{-1} may arise from ν(C−O) of carbon black surfaces.

More importantly, Figure 5 shows the distinct feature of bridge-bonded CO (CO_B) on Pd nanoparticle surfaces, as can be seen from the gradually increased shoulder peaks from ca. 1830 to 1870 cm^{-1},[40] despite the fact that no CO gas was detected by GC. According to our previous study,[28,29] the slow accumulation of low-coverage CO_{ad} at Pd surfaces arises mainly from the reduction of the dehydrogenation product CO_2 rather than direct dehydration of FA. To further address the role of CO_{ad}, a control experiment was carried out by adding CO-saturated FA-SF solution to 100 mg of Pd/C-$NaBH_4$ catalyst. As a result, less than 1 mL of reforming gas was generated in 3 h, demonstrating fatal poisoning of catalytic sites by adsorbed CO.

Along this line, Figure 6 illustrates the time-evolved frequency of the $\nu(CO_B)$ band on Pd/C-$NaBH_4$ and Pd-B/C

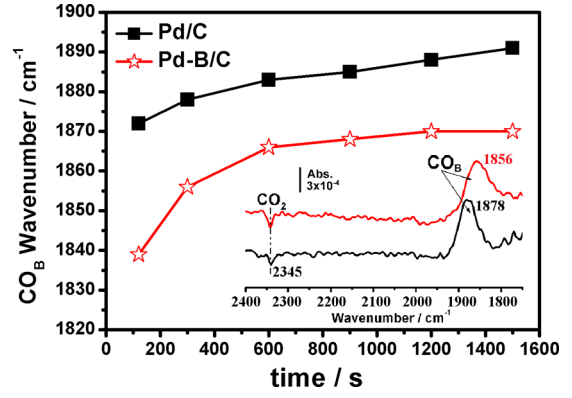

Figure 6. Time-course of changing C−O stretching frequency of bridge-bonded CO (CO_B) on Pd/C and Pd-B/C catalysts. The inset spectra were recorded 300 s after FA-SF injection, using the single-beam spectrum acquired at 60 s as the reference spectrum.

taken from a series of ATR-IR spectra recorded in 1.1 M FA + 0.8 M SF, and the inset shows the ATR-IR spectra at 300 s after spectral subtraction of the bulk FA signals acquired at 60 s. A lower frequency of the $\nu(CO_B)$ band on Pd-B/C throughout ATR-IR measurements was observed, suggesting a lower CO_{ad} coverage or an enhanced anti-poisoning ability, given that the $\nu(CO_{ad})$ band center frequency increases with CO coverage on metal surfaces. In other words, slower CO_{ad} accumulation may

dx.doi.org/10.1021/ja5008917 | J. Am. Chem. Soc. 2014, 136, 4861−4864

at least partly account for enhanced Pd-catalyzed hydrogen production from a FA-SF solution with Pd-B/C. Furthermore, the Pd-B nanoparticles have a slightly expanded Pd lattice, which is similar to the effective Pd/Au(Ag) nanoalloy and Ag@Pd nanoparticles used in the literature.[17,21,23] This structural change may increase the adsorption of formate ions, which in turn may induce an H-down orientation of FA molecules approaching Pd surfaces,[36,37] enabling FA dehydrogenation to occur at a lower activation energy. The above correlations could be used to guide the rational design of new Pd-based catalysts. Last but not least, this work demonstrates that efficient Pd-based catalysts for hydrogen production can now be achieved without the inclusion of another noble metal. Future work will aim to understand the higher activity of Pd-B catalyst via DFT calculations and to optimize the size of Pd-B nanoparticles and the structure of the support.

In summary, we present an initial report on metalloid-doped Pd nanocatalysts for efficient H_2 production from aqueous FA-SF at ambient conditions. The TOF reaches 1184 h^{-1} at 30 °C on Pd-B/C and is ca. 3 times higher than that on Pd/C. Furthermore, CO_{ad} accumulation on Pd surfaces during hydrogen generation is detected by high-sensitivity ATR-IR measurement, even though CO content in the gas is below 1 ppm, if any. Lower coverage of CO on Pd-B/C catalyst as compared to Pd/C correlates with the enhanced hydrogen production on the former. The effective metalloid doping coupled with high sensitivity ATR-IR measurements offers a promising approach to designing new catalysts for efficient dehydrogenation of formic acid.

■ ASSOCIATED CONTENT

Supporting Information

Experimental details, additional material characterization, and evaluation. This material is available free of charge via the Internet at http://pubs.acs.org.

■ AUTHOR INFORMATION

Corresponding Author

wbcai@fudan.edu.cn

Notes

The authors declare no competing financial interest.

■ ACKNOWLEDGMENTS

This work is supported by NSFC (Nos. 21073045 and 21273046), SMCST (Nos. 11JC140200 and 08DZ2270500). We appreciate Profs. Minghua Qiao and Weilin Dai, and Dr. Chao Wen for GC measurements.

■ REFERENCES

(1) Boddien, A.; Loges, B.; Gärtner, F.; Torborg, C.; Fumino, K.; Junge, H.; Ludwig, R.; Beller, M. *J. Am. Chem. Soc.* **2010**, *132*, 8924.
(2) Yadav, M.; Xu, Q. *Energy Environ. Sci.* **2012**, *5*, 9698.
(3) Whipple, D. T.; Kenis, P. J. A. *J. Phys. Chem. Lett.* **2010**, *1*, 3451.
(4) Grasemann, M.; Laurenczy, G. *Energy Environ. Sci.* **2012**, *5*, 8171.
(5) Capon, A.; Parsons, R. *J. Electroanal. Chem.* **1973**, *45*, 205.
(6) Gu, X.; Lu, Z.-H.; Jiang, H.-L.; Akita, T.; Xu, Q. *J. Am. Chem. Soc.* **2011**, *133*, 11822.
(7) Solymosi, F.; Koos, A.; Liliom, N.; Ugrai, I. *J. Catal.* **2011**, *279*, 213.
(8) Chen, A.; Holt-Hindle, P. *Chem. Rev.* **2010**, *110*, 3767.
(9) Cuesta, A.; Cabello, G.; Osawa, M.; Gutierrez, C. *ACS Catal.* **2012**, *2*, 728.
(10) Ojeda, M.; Iglesia, E. *Angew. Chem., Int. Ed.* **2009**, *48*, 4800.
(11) Bi, Q. Y.; Du, X. L.; Liu, Y. M.; Cao, Y.; He, H. Y.; Fan, K. N. *J. Am. Chem. Soc.* **2012**, *134*, 8926.
(12) Zhou, X. C.; Huang, Y. J.; Xing, W.; Liu, C. P.; Liao, J. H.; Lu, T. H. *Chem. Commun.* **2008**, 3540.
(13) Bulushev, D. A.; Jia, L. J.; Beloshapkin, S.; Ross, J. R. H. *Chem. Commun.* **2012**, *48*, 4184.
(14) Jones, S.; Qu, J.; Tedsree, K.; Gong, X. Q.; Tsang, S. C. E. *Angew. Chem., Int. Ed.* **2012**, *51*, 11275.
(15) Wang, Z. L.; Yan, J. M.; Wang, H. L.; Ping, Y.; Jiang, Q. *Sci. Rep.* **2012**, *2*, 598.
(16) Mori, K.; Dojo, M.; Yamashita, H. *ACS Catal.* **2013**, 1114.
(17) Huang, Y. J.; Zhou, X. C.; Yin, M.; Liu, C. P.; Xing, W. *Chem. Mater.* **2010**, *22*, 5122.
(18) Zhou, X. C.; Huang, Y. J.; Liu, C. P.; Liao, J. H.; Lu, T. H.; Xing, W. *Chemsuschem* **2010**, *3*, 1379.
(19) Gu, X. J.; Lu, Z. H.; Jiang, H. L.; Akita, T.; Xu, Q. *J. Am. Chem. Soc.* **2011**, *133*, 11822.
(20) Wang, Z. L.; Yan, J. M.; Ping, Y.; Wang, H. L.; Zheng, W. T.; Jiang, Q. *Angew. Chem., Int. Ed.* **2013**, *52*, 4406.
(21) Zhang, S.; Metin, O.; Su, D.; Sun, S. H. *Angew. Chem., Int. Ed.* **2013**, *52*, 3681.
(22) Metin, O.; Sun, X. L.; Sun, S. H. *Nanoscale* **2013**, *5*, 910.
(23) Tedsree, K.; Li, T.; Jones, S.; Chan, C. W. A.; Yu, K. M. K.; Bagot, P. A. J.; Marquis, E. A.; Smith, G. D. W.; Tsang, S. C. E. *Nat. Nanotechnol.* **2011**, *6*, 302.
(24) Fellay, C.; Yan, N.; Dyson, P. J.; Laurenczy, G. *Chem.—Eur. J.* **2009**, *15*, 3752.
(25) Fellay, C.; Dyson, P. J.; Laurenczy, G. *Angew. Chem., Int. Ed.* **2008**, *47*, 3966.
(26) Ting, S. W.; Cheng, S. A.; Tsang, K. Y.; van der Laak, N.; Chan, K. Y. *Chem. Commun.* **2009**, 7333.
(27) Kakuta, S.; Abe, T. *ACS Appl. Mater. Interfaces* **2009**, *1*, 2707.
(28) Wang, J. Y.; Zhang, H. X.; Jiang, K.; Cai, W. B. *J. Am. Chem. Soc.* **2011**, *133*, 14876.
(29) Zhang, H. X.; Wang, S. H.; Jiang, K.; Andre, T.; Cai, W. B. *J. Power Sources* **2012**, *199*, 165.
(30) Zhu, Q.-L.; Tsumori, N.; Xu, Q. *Chem. Sci.* **2014**, *5*, 195.
(31) Martis, M.; Mori, K.; Fujiwara, K.; Ahn, W.-S.; Yamashita, H. *J. Phys. Chem. C* **2013**, *117*, 22805.
(32) Ping, Y.; Yan, J.-M.; Wang, Z.-L.; Wang, H.-L.; Jiang, Q. *J. Mater. Chem. A* **2013**, *1*, 12188.
(33) Wang, J. Y.; Kang, Y. Y.; Yang, H.; Cai, W. B. *J. Phys. Chem. C* **2009**, *113*, 8366.
(34) Carenco, S.; Portehault, D.; Boissière, C.; Mézailles, N.; Sanchez, C. *Chem. Rev.* **2013**, *113*, 7981.
(35) Wakisaka, M.; Mitsui, S.; Hirose, Y.; Kawashima, K.; Uchida, H.; Watanabe, M. *J. Phys. Chem. B* **2006**, *110*, 23489.
(36) Wang, H. F.; Liu, Z. P. *J. Phys. Chem. C* **2009**, *113*, 17502.
(37) Peng, B.; Wang, H. F.; Liu, Z. P.; Cai, W. B. *J. Phys. Chem. C* **2010**, *114*, 3102.
(38) Gao, W.; Keith, J. A.; Anton, J.; Jacob, T. *J. Am. Chem. Soc.* **2010**, *132*, 18377.
(39) Joo, J.; Uchida, T.; Cuesta, A.; Koper, M. T. M.; Osawa, M. *J. Am. Chem. Soc.* **2013**, *135*, 9991.
(40) Mojet, B. L.; Ebbesen, S. D.; Lefferts, L. *Chem. Soc. Rev.* **2010**, *39*, 4643.

Supporting Information

B-doped Pd Catalyst: Boosting Room-Temperature Hydrogen Production from Formic Acid-Formate Solutions

Kun Jiang,[a] Ke Xu,[a] Shouzhong Zou[b] and Wen-Bin Cai[a]*

[a] Shanghai Key Laboratory of Molecular Catalysis and Innovative Materials, Collaborative Innovation Center of Chemistry for Energy Materials, Department of Chemistry, Fudan University, Shanghai 200433, China

[b] Department of Chemistry and Biochemistry, Miami University, Oxford, OH 45056, USA;

*Corresponding author. E-mail: wbcai@fudan.edu.cn

Experimental

Catalyst Syntheses

Carbon supported Pd-B catalyst was prepared through a wet chemical synthesis with dimethylamine borane (DMAB) as the reducing agent. Typically, 25 mg of NH_4F, 125 mg of H_3BO_3 and 157 μmol of Na_2PdCl_4 was mixed in 20 mL of Milli-Q H_2O (18.2MΩ•cm), and kept under vigorous stirring with high-purity N_2 bubbling for 15 min. The pH was adjusted to ca. 9 with aqueous ammonia. Then, 318 mg of Vulcan XC-72 carbon was added to form carbon slurry and further sonicated for 30 min. Under vigorous stirring, 20 mL of freshly prepared ice-cold 0.1 M DMAB aqueous solution was dropwisely added to the suspension at 0.5 mL/min controlled by a peristaltic pump. The whole reduction procedure was carried out in an ice-water bath for 2 h. The resulted suspension was further stirred at 30 °C for 2 h. Finally, it was filtered, washed with copious amounts of Milli-Q water and vacuum dried at 70 °C overnight.

Carbon supported Pd catalyst was prepared in aqueous solution by $NaBH_4$ impregnation-reduction method, noted as Pd/C-$NaBH_4$. Typically, 157 μmol of Na_2PdCl_4 and 318 mg of Vulcan XC-72 Carbon were added into 50 mL of Milli-Q water. Such a mixture was sonicated for 30 min and stirred for another 2 h, then the solution pH was adjusted to ca. 9-10 with aqueous ammonia. 15 mL of 0.05 M Na_2CO_3 containing 30 mg of $NaBH_4$ was dropwisely added to the suspension at 0.5 mL/min controlled by a peristaltic pump. The resulting suspension was further stirred at room temperature for 2 h, then filtered and washed with copious amounts of Milli-Q water, and eventually vacuum-dried at 70 °C overnight.

To further exclude any boron doping, HCOONa was used as the reducing agent instead of the commonly used $NaBH_4$ to synthesize the other Pd/C catalyst, noted as Pd/C-HCOONa. The synthetic procedure mainly followed Wang *et al.*'s method[1] with some modification. Typically, 157 μmol of Na_2PdCl_4 and 318 mg of Vulcan XC-72 Carbon were added into 50 mL of Milli-Q water and sonicated for 30 min. Then, 20 mL of mixed aqueous solution containing 1.1 M formic acid (FA), 0.8 M sodium formate (SF) and 0.03 M citric acid was fast injected into the slurry. The resulting suspension was further stirred at 30 °C for 3 h, then filtered and washed with a copious amount of Milli-Q water, and eventually vacuum-dried at 70 °C overnight. Pd loading for all the catalysts was set to be 5 wt.%.

Material Characterization

The chemical compositions of Pd-based catalysts were analysed by inductively coupled plasma-atomic emission spectroscopy (ICP-AES) on a Thermo Elemental IRIS Intrepid. The crystalline structures were examined by X-ray diffraction (XRD) on a D8 Advance and Davinci Design X-ray diffractometer with the Cu Kα radiation from 30° to 90°, and the particle sizes and dispersions were characterized by (high resolution) transmission electron microscopy (HR-TEM) on a JEOL JEM-2100F microscope. The surface information of desired nanocatalysts was analysed by X-ray photoelectron spectroscopy (XPS), carried out on a Perkin-Elmer PHI-5000C ESCA system equipped with a hemispherical electron energy analyser, using a monochromatic Mg Kα radiation (1253.6 eV). The binding energies were

calibrated by referencing to the C 1s peak at 284.6 eV.

Catalyst Evaluation

The hydrogen production from FA-SF solution was carried out in a 25-mL flask at 30 °C controlled by a Heidolph MR Hei-Standard Magnetic Stirrer, and the production rate of reforming gas (H_2 + CO_2) was measured by a gas burette. Typically, 100 mg of catalyst (ca. 5 mg of Pd) was first placed in the flask, then 10 mL of FA solution containing 11 mmol of FA and 8 mmol of SF was injected quickly. The reforming gas composition was analysed by a GC9560 gas chromatograph (GC) with a TDX-01 packed column (L = 2 m) connected to a thermal conductivity detector (TCD). The content of CO (if any) was analysed by a gas chromatography equipped with a methanator and a flame ionization detector (FID) whose detection limit for CO is 1 ppm. A mixed gas consisting of H_2, CO, CH_4, CO_2, N_2 and Ar was used as the reference.

***in situ* ATR-IR Measurements**

The ATR-IR measurement was run on a Pd-based/C catalyst layer covered on Au film chemically deposited on the basal plane of a hemicylindrical Si prism using a Varian 3100 FT-IR Excalibur spectrometer equipped with an MCT detector, at a spectral resolution of 8 cm^{-1} with unpolarized IR radiation at an incidence angle of ca. 65°. A catalyst ink was first prepared by mixing 1 mL of C_2H_5OH, 2 mg of catalyst and 120 μL of Nafion (5 wt.%, Aldrich), sonicated for 1 h. Then 100 μL of this ink was transferred onto an electrochemically polished Au film via a pipette. All the spectra are shown in the absorbance unit as -log (I/I_0), where I and I_0 represent the intensities of the reflected radiation of the sample and reference spectra, respectively. Experimental details including chemical deposition of the Au films, preparation of the catalyst ink and the catalyst overlayer on Au films, setup of the ATR cell etc., can be found elsewhere.[2-4]

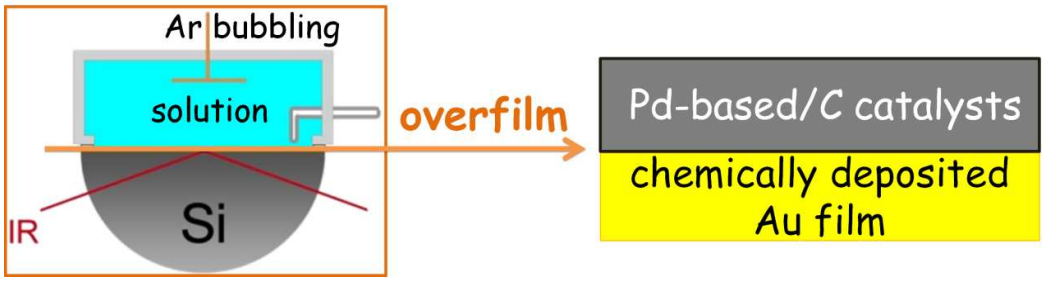

Scheme S1. Setup of an ATR cell with a catalyst covered on Au/Si. Vigorous Ar bubbling was carried out throughout IR measurements to mimic practical stirring condition.

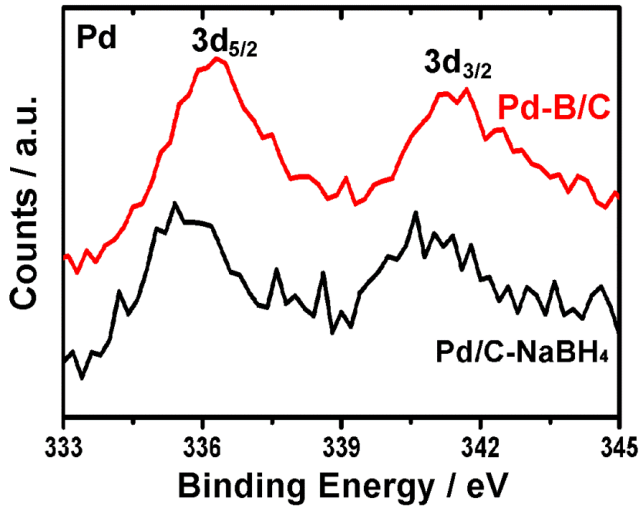

Figure S1. Core level XPS spectra in Pd 3d regions of as-prepared Pd/C-$NaBH_4$ and Pd-B/C catalysts. A striking binding energy shift of 0.9 eV for Pd^0 $3d_{5/2}$ is clearly observed on Pd-B/C as compared to Pd/C-$NaBH_4$, corresponding to the charge transfer effect ascribed to efficient boron doping from DMAB.

Traditionally, the increased core-level binding energy of a metal element in an XPS spectrum sugguests a loss of electrons of the metal (or M^0 to M^{z+}). However, as for nanoalloys the electron transfer between two components is more complicated for analysis. In an impressive report on XPS characterization of Pt-Ru and Pt-Co alloys by M. Watanabe *et al.*,[5] the positive shift of Pt $4f_{7/2}$ binding energy versus the Fermi level was ascribed to the electron transfer from Ru (Co) to Pt.

In contrast, electron transfer from Pd to Cu was proposed by another group for Pd-Cu alloy[6] in explaining the positively shifted binding energy of Pd $3d_{5/2}$ after alloyment with Cu, based on the traditional way to explain the XPS results for different valences of a metal element.

Furthermore, in a latest critical review on metal borides,[7] the electron transfer from B to M for metal-rich borides (MB_x, $x \leq 2$) is commonly accepted. On the basis of the above arguments and our XPS result, we tend to suggest that electron transfer from B to Pd should occur in Pd-B/C with a low B content.

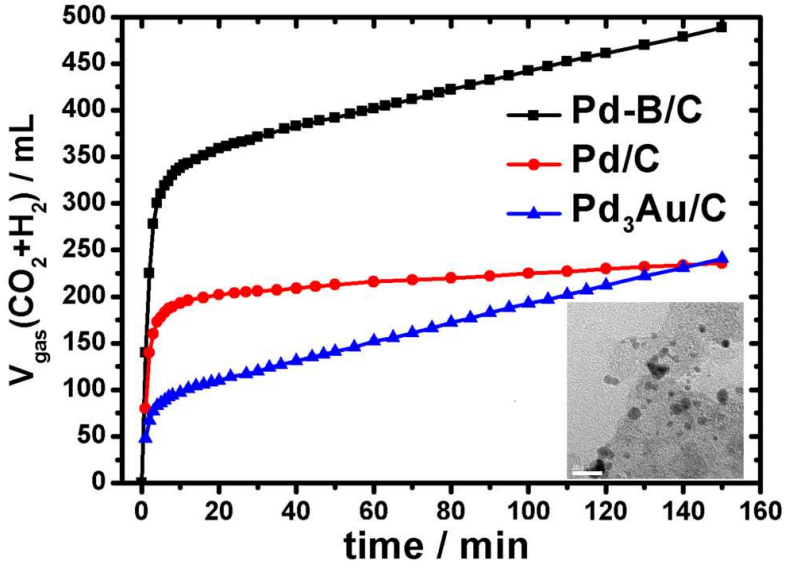

Figure S2. Time-course reforming gas generated from 5 mL of 9.9 M FA + 3.3 M SF in the presence of 120 mg Pd-B/C, Pd/C-$NaBH_4$ or Pd_3Au/C at 92 °C. Inset is the TEM image of as-prepared Pd_3Au/C with a 20 nm scale bar. The experimental conditions for H_2 production and the preparation of Pd_3Au/C are the same as Ref. 13 in the main text except for a lower metal loading of 5 wt.% Pd, for a better comparison with the reported Pd-M/C (M = Au, Ag, Cu etc.).[8] The gas generation rate on Pd-B/C is comparable to the Pd_3Au/C at a given Pd usage (Au usage is not taken into account).

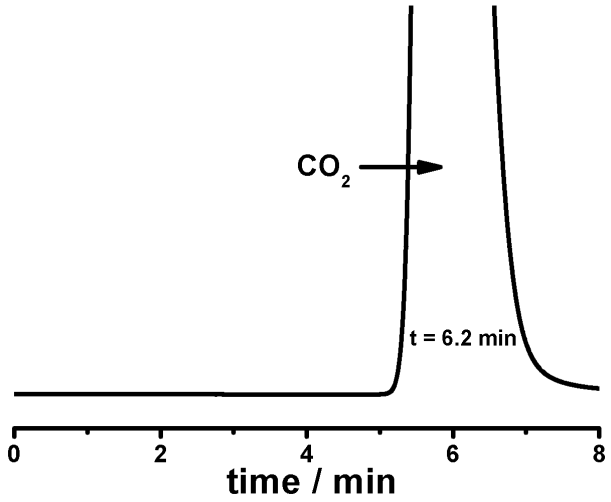

Figure S3. Gas chromatogram of the room-temperature generated reforming gas recorded on a GC-FID equipped with a methanator. The absence of CO signal at about 1.2 min suggests that the CO content is below the instrumental detection limit of 1 ppm.

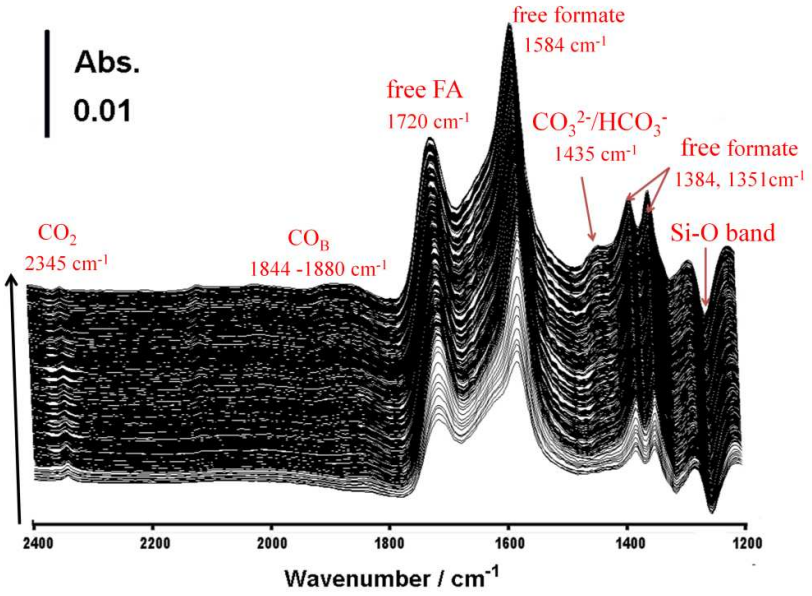

Figure S4. Time-evolved ATR-IR spectra of Pd/C coated Au film/Si prism recorded after injecting a pre-mixed solution of 1.1 M FA + 0.8 M SF to the spectral cell. Reference spectrum was recorded in air before the injection, and the acquisition time for each single-beam spectrum is 5 s.

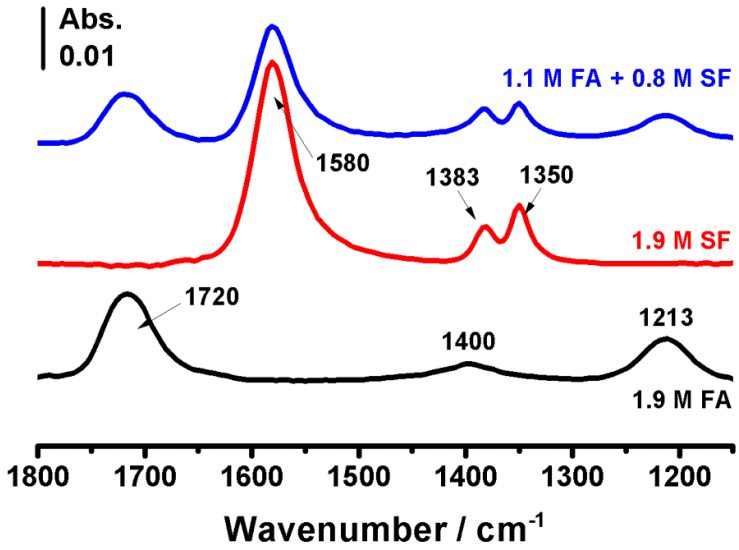

Figure S5. ATR-IR spectra of formic acid (black), sodium formate (red) and their mixture (blue) adsorbed on bare Si prism, reference spectrum was recorded in air before the injection.

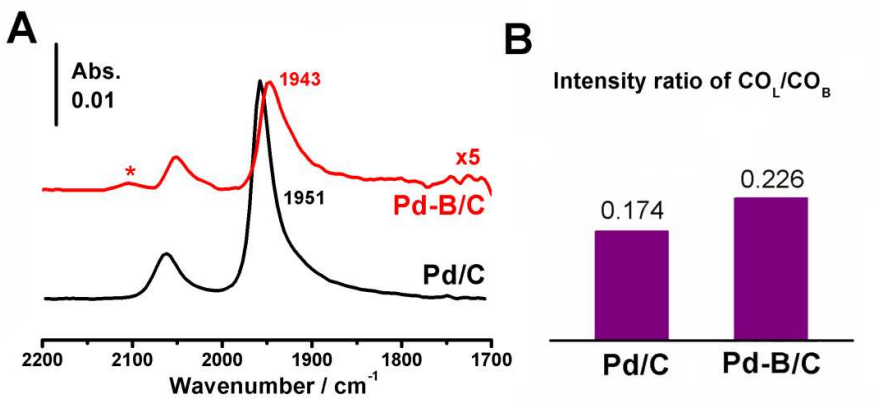

Figure S6. (A) ATR-IR spectra of CO adsorbed on Pd/C and Pd-B/C respectively coated on Au/Si in CO-saturated $HClO_4$-$NaClO_4$ solution (ca. pH 3.5), CO adsorbed on Au underfilm was indicated by *. Reference spectra were recorded prior to bubbling CO. (B) The intensity ratio of $\nu(CO_L)$ to $\nu(CO_B)$ on Pd/C-$NaBH_4$ and Pd-B/C. The decreased peak intensity on Pd-B/C may come from a smaller exposed Pd surface area (a larger size 4.1 nm vs 2.2 nm) and a lower CO coverage. The latter is further indicated by the lower frequencies of the $\nu(CO_L)$ and $\nu(CO_B)$ bands and increased ratio of the $\nu(CO_L)$ band intensity to the $\nu(CO_B)$ band intensity.

References

(1) Wang, Z. L.; Yan, J. M.; Wang, H. L.; Ping, Y.; Jiang, Q. *Sci. Rep.* **2012**, *2*, 598.

(2) Yan, Y. G.; Li, Q. X.; Huo, S. J.; Ma, M.; Cai, W. B.; Osawa, M. *J. Phys. Chem. B* **2005**, *109*, 7900.

(3) Zhang, H. X.; Wang, S. H.; Jiang, K.; Andre, T.; Cai, W. B. *J. Power Sources* **2012**, *199*, 165.

(4) Jiang, K.; Cai, W. B. *Appl. Catal., B* **2014**, *147*, 185.

(5) Wakisaka, M.; Mitsui, S.; Hirose, Y.; Kawashima, K.; Uchida, H.; Watanabe, M. *J. Phys. Chem. B* **2006**, *110*, 23489.

(6) Hu, S.; Ha, S.; Scudiero, L. *Electrochim. Acta* **2013**, *105*, 362.

(7) Carenco, S.; Portehault, D.; Boissière, C.; Mézailles, N.; Sanchez, C. *Chem. Rev.* **2013**, *113*, 7981.

(8) Zhou, X. C.; Huang, Y. J.; Xing, W.; Liu, C. P.; Liao, J. H.; Lu, T. H. *Chem. Commun.* **2008**, 3540.